Quantifying Anisotropic Solute Transport in Protein Crystals Using 3-D Laser Scanning Confocal Microscopy Visualization

A. Cvetkovic,[1] A. J. J. Straathof,[1] D. N. Hanlon,[2] S. van der Zwaag,[3] R. Krishna,[4] L. A. M. van der Wielen[1]

[1]Department of Biotechnology, Delft University of Technology, Julianalaan 67, 2628 BC Delft, The Netherlands; telephone: + 31-15-2782361; fax: + 31-15-2782355; e-mail: L.A.M.vanderWielen@tnw.tudelft.nl
[2]Netherlands Institute for Metals Research, Rotterdamseweg 137, 2628 AL Delft, The Netherlands
[3]Laboratory for Materials Science, Delft University of Technology, Rotterdamseweg 137, 2628 AL Delft, The Netherlands
[4]Department of Chemical Engineering, University of Amsterdam, Nieuwe Achtergracht 166, 1018 WV Amsterdam, The Netherlands

Received 24 July 2003; accepted 28 October 2003

Published online 30 March 2004 in Wiley InterScience (www.interscience.wiley.com). DOI: 10.1002/bit.20067

Abstract: The diffusion of a solute, fluorescein into lysozyme protein crystals has been studied by confocal laser scanning microscopy (CLSM). Confocal laser scanning microscopy makes it possible to non-invasively obtain high-resolution three-dimensional (3-D) images of spatial distribution of fluorescein in lysozyme crystals at various time steps. Confocal laser scanning microscopy gives the fluorescence intensity profiles across horizontal planes at several depths of the crystal representing the concentration profiles during diffusion into the crystal. These intensity profiles were fitted with an anisotropic model to determine the diffusivity tensor. Effective diffusion coefficients obtained range from 6.2×10^{-15} to 120×10^{-15} m^2/s depending on the lysozyme crystal morphology. The diffusion process is found to be anisotropic, and the level of anisotropy depends on the crystal morphology. The packing of the protein molecules in the crystal seems to be the major factor that determines the anisotropy. © 2004 Wiley Periodicals, Inc.

Keywords: CLSM; protein crystals; diffusion; anisotropy

INTRODUCTION

Protein crystals are characterized by their mesoporic structure, with a porosity content ranging from 25–60% (Matthews, 1968), pore diameters in the range of 0.5–10 nm (Matthews, 1968; Vilenchik et al., 1998), a pore volume of 0.9–3.6 mL/g (Vilenchik et al., 1998), and a total surface area of 800–3000 m^2/g (Morozov et al., 1995; Vilenchik et al., 1998). This makes them perfect candidates for studying the mechanisms by which ligands bind to protein molecules and catalyze reactions, and to study transport processes that might cause differences between the properties of crystalline and dissolved proteins (Rupley, 1969). Cross-linked protein crystals may find a broad range of applications in biocatalysis (Margolin and Navia, 2001; St Clair and Navia, 1992), medical formulations (Margolin and Navia, 2001), detergents (Margolin and Navia, 2001), in separation process such as chromatography (Vilenchik et al., 1998), and as biosensors (Morozov and Morozova, 1992).

The understanding of transport rates inside the pores of protein crystals is crucial for several applications. When applied in biocatalytic processes, there are three major factors that control enzymatic activity in the crystalline state: the size of the crystal, the size of the substrate, and the conformation of the enzyme in the crystal. In many cases, the full activity of an enzyme crystal cannot be achieved because of mass-transfer limitations (Doscher and Richards, 1963; Genzel et al., 1976; Westbrook and Sigler, 1984). The empirically determined critical crystal thickness below which diffusional limitations are not significant (Sluyterman and de Graaf, 1969) depends on the diffusion coefficient of the substrate in the crystal, on the kinetic parameters of the enzyme, and on the enzyme concentration. When protein crystals are applied in the area of chromatography (Pastinen et al., 1998, 2000; Vilenchik et al., 1998), good separation capability may be provided by at least three different mechanisms: size exclusion, adsorption, and diffusion. All, to different extents, depend on the transport limitations in the system. Using purely empirical factors, such as critical crystal thickness, will not provide understanding of the separation capability, so fundamental knowledge of solute diffusion in the protein crystals will be required.

Experimental methods used for the determination of transport processes in protein crystals can be divided into indirect and direct methods. For the indirect methods, concentration changes of solutes in the protein crystals are

Correspondence to: L. A. M. van der Wielen

Contract grant sponsor: Netherlands Foundation for Scientific Research-Chemical Sciences (NWO-CW)

determined on the basis of concentration changes in the bulk liquid phase in which the crystals are immersed. Such data do not provide information about the concentration distribution within the crystal, the transport mechanisms across the outer surface, into the pores of the crystal, nor about the local driving forces of the process.

Direct methods, on the other hand, use concentrations measured in the protein crystal. Granick (1942) determined transport parameters of solutes in protein crystals qualitatively by monitoring the overall color variations in a guinea pig oxyhemoglobin crystal due to the penetration of K-ferricyanide. The quantitative determination of transport parameters commenced with the introduction of X-ray fluorescence measurements (Bishop and Richards, 1968), video absorbance spectroscopy (O'Hara et al., 1995), and quantitative fluorescence microscopy (Velev et al., 2000). These analytical methods allow the determination of accumulated concentration profiles through the protein crystal. Such data can be used to calculate the transport process in a crystal, but a spherical or cylindrical geometry have to be assumed. In reality, protein crystals have much more complex macroscopic morphologies (Fig. 1) and, furthermore, their mesoscopic pore structure is far from being isotropic (Vilenchik et al., 1998).

In order not to be restricted to isotropic structures, the transport processes in protein crystals have been determined using sliced sections of protein crystals obtained by using a microtome (Botin and Morozov, 1985; Kachalova et al., 1995). For each section the variation of the concentration of solutes can be determined applying analytical methods such as spectrophotometry (Botin and Morozov, 1985) or X-ray fluorescence (Kachalova et al., 1995). The major drawbacks of these methods are that: (1) the crystal layers might be damaged by the cutting process, consequently leading to erroneous results, (2) the variation of the concentration can only be determined as a function of the position in the crystal and not as a function of time, (3) slicing is very difficult and time consuming. To date, the experimental techniques allow either the description of the transport process as a function of time or as a function of the position, but not as a function of both simultaneously.

In this article, an experimental method is introduced describing simultaneously the spatial and the temporal resolution of solute distribution in protein crystals. This method employs confocal laser scanning microscopy (CLSM), which has previously been applied for the visualization of the transport process of dyes and dye-targeted molecules in various materials (Ahmed and Pyle, 1999; Benda et al., 2003; Kim et al., 1996; Linden et al., 1999; Ljunglof and Thommes, 1998; Ljunglof et al., 2000; Lowry et al., 2002; Malmsten et al., 1999; Rademann et al., 2001; Reichert et al., 2002; Song et al., 2000). The essential advantage of CLSM is its ability to discriminate between the lights from the desired focal plane and unwanted out-of-focus light that limits the application of a normal light microscope to obtain three-dimensional (3-D) images of transparent objects. Incident light at discrete wavelengths excites fluorescent solute molecules, which enter the crystal from the surrounding solution. An illumination source, a laser, is directed through an illumination pinhole (Fig. 2). The light coming through this pinhole is imaged via a beam splitter into a focal spot within the sample. The fluorescent light is collected and focused onto another confocal pinhole, which is placed so that the image of the focal plane falls exactly onto this pinhole. Hence, the two pinholes are confocal to each other. If scattering of the incident beam causes fluorescence outside of the plane in the focus, only the fluorescence from the focal plane is able to pass through the confocal pinhole. The thickness of a layer in focal plane depends on the diameter of the pinhole, the numerical aperture of the objective lens, and the wavelength of the applied laser light. The detection of the resulting fluorescence signal provides a horizontal two-dimensional (2-D) image of the spatial distribution of solute within the crystal. Vertical displacement of the sample yields a series of optical section images describing the distribution

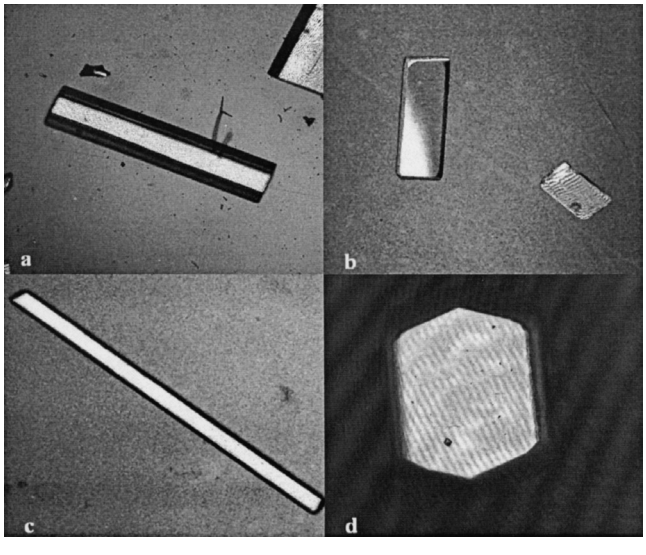

Figure 1. Different structures of lysozyme crystals used in the present study: (a) triclinic (P1), (b) monoclinic ($P2_1$), (c) orthorhombic ($P2_12_12_1$), (d) tetragonal ($P4_12_12_1$).

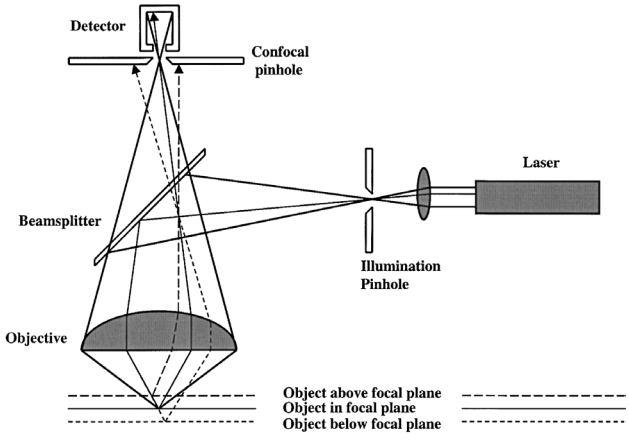

Figure 2. Working principle of the confocal laser scanning microscope.

of fluorescent light intensities, and therefore, the solute distribution, across a series of horizontal cross sections. Since the series of these optical section images are obtained in a digital form, several successive optical sections can be postprocessed to construct a 3-D image of the crystal. Modern CLSM systems that are equipped with sophisticated computer control systems and fast digital image capture devices allow in situ observation of the variation of solute distribution, in all three spatial directions and its development with time, simultaneously.

Here we report experimental data and preliminary quantitative analysis on the transport process of sodium fluorescein in lysozyme crystal. Chicken egg-white lysozyme has been chosen as a model protein because the crystals thereof can be obtained easily and reproducibly, and also because the properties and morphologies of these crystals are well known.

MATERIALS AND METHODS

Crystallization of Lysozyme Crystals

Chicken egg-white lysozyme was obtained from Sigma (Prod. no. L-6876; 95% purity; M_w = 14307 g/mol) and was used without further purification. Four different structures of lysozyme crystals (Table I) were grown. Triclinic (P_1) and monoclinic ($P2_1$) lysozyme crystals were grown according to the method developed by Steinrauf (1959) in the solution containing 3% and 2% (w/v) sodium nitrate, respectively, and 1% (w/v) lysozyme at a pH of 4.5. Tetragonal lysozyme crystals ($P4_32_12_1$) were grown according to a modification of the procedure described by Feher and Kam (1985). Crystallization solution was prepared from 0.1 mol/L sodium acetate buffer with around 6% (w/v) of sodium chloride and 1.5% (w/v) lysozyme at a pH of 4.5. Orthorhombic lysozyme crystals ($P2_12_12_1$) were grown using the same procedure as for the crystallization of the tetragonal structure but their pH was adjusted to 10 by the addition of 1 mol/L sodium hydroxide.

After the preparation of the crystallization solution, this solution was filter-sterilized using Schleicher & Schuell (Germany) syringe filters with a cut-off value of 200 nm. All crystals were grown from the filtered solution by the batch method for 2–14 days in a closed glass or plastic vials and tubes. Properties of the crystal are presented in Table I.

Preparation of Fluorescein Solutions

Sodium fluorescein (Sigma, Prod. no. F-6377; M_w = 376.85 g/mol) is a fluorescent dye with a maximum emission at 525 nm if excited by incident light at a wavelength of 490 nm.

Fluorescein deteriorates when exposed for a long time (6 days) to daylight (Diehl, 1987). Therefore, the fluorescein solutions were stored and the experiments were done in a dark room. Fresh solutions were used for all experiments. The absorbance of the fluorescein solution, kept in a dark place, was checked and no change was observed over 3 weeks time. Additionally, only a 0.7% decrease in fluorescence intensity could be detected if a fluorescein solution was exposed to laser light during 12 h, indicating that photodestruction was negligible.

Mother liquid solutions were filtered using Schleicher & Schuell (Germany) syringe filters with a cut-off value of 200 nm and concentrated solution of sodium fluorescein (2 g/L) was added until the desired concentration of 0.003 g/L was reached. Prior to the experiment, density (DMA 48, Anton Paar), pH, and the lysozyme content of starting solution had been determined. The lysozyme content was determined by measuring absorption (Pharmacia, Ultrospec III) at 281 nm.

Confocal Laser Scanning Microscopy

A Leica TCS SP Confocal Laser Scanning Microscope (Leica Microsystems, Heidelberg, Germany) was used in the fluorescence mode. Its argon laser produces light with wavelengths in the range of 458–514 nm. For our experiments the samples were excited with laser at a wavelength of 488 nm and light emitted in the 500–600 nm wavelength range was collected.

A diffusion cell with an operational compartment of 22 mm diameter and 4 mm height surrounded by a separate annular compartment of 3-mm width and 4-mm height was used in the experiments. The cell was completely filled with 0.003 g/L sodium fluorescein solution. A uniformly shaped protein crystal was selected and added. The solution was protected by a cover glass, so that evaporation, if any, oc-

Table I. Characteristics of the lysozyme crystal structures and diffusion parameters (including 95% confidence interval) estimated for fluorescein transport in lysozome crystals. The pH indicates not only the crystallization pH but also that of the CLSM experiments.

Crystal structure	PDB name	Precipitant	Density[a] kg/m^3	pH	Solvent[b] content (v/v)	$D_{oe} \times 10^{15}$ m^2/s	$D_x \times 10^{15}$ m^2/s	$D_y \times 10^{15}$ m^2/s	$D_z \times 10^{15}$ m^2/s
Tetragonal	1HEL	NaCl	1242	4.4–4.6	0.42	123 ± 5.7	53 ± 0.8	79 ± 11	190 ± 7.1
Orthorhombic	1AKI	NaCl	1304	8.8–9.2	0.44	16 ± 0.5	7.4 ± 0.8	304 ± 17	19 ± 1.1
Monoclinic	1LZH	$NaNO_3$	1239	5.3–5.4	0.36	20 ± 1.0	10 ± 0.7	n.d.	18 ± 0.6
Triclinic	4LZT	$NaNO_3$	1269	4.6–4.8	0.33	6.2 ± 0.1	n.d.[c]	8.6 ± 0.4	12 ± 1.3

[a]Steinrauf, 1959.
[b]solvent content was calculated based on equation given in McRee (1999).
[c]n.d. = not determined.

curred only in the annular compartment. The temperature of the environment was maintained at 16°C to prevent heating of the diffusion cell during scanning process.

Prior to the CLSM measurements, the diffusion cell was gently shaken for 30–40 s. The solution surrounding the crystal was not agitated during the experiments to prevent any crystal damage.

The confocal images were obtained with an HC PL Fluotar 10.0 × 0.30 N.A. BD and an HC PL Fluotar 20.0 × 0.50 N.A. BD objective lens. The box size of the digital images was 512 × 512 pixels, corresponding to a 1 × 1 mm or 0.5 × 0.5 mm sample area. In some experiments the image was zoomed 2 or 4 times, which resulted in a pixel size in the range of 0.244 × 0.244 μm to 1.953 × 1.953 μm. Images were stored at 8-bit resolution. The Leica TCS achieves a lateral resolution of 322 nm and a corresponding axial resolution of 2540 nm. The power of the laser was kept low (9%). The size of the detection pinhole and the contrast were kept constant for all experiments.

Scans were made perpendicular to the laser beam starting from a horizontal plane at the base of the crystal and at constant vertical intervals up to the top surface of the crystal. Each of the 2-D scan data sets shown in this study represents an average of four scans.

Typically, in the first 20 min of exposure, the image was taken every 2 min. Then, the interval between scans was increased to 5 and 15 min. After 4 h, the time step was increased again such that images were scanned every 1 h. The total duration of the experiment was between 24–72 h depending on the size and structure of used crystal.

The intensity profiles in x and y directions were directly extracted from the confocal 2-D images using Matlab (Natick, MA). For every confocal image the same procedure was applied. A crystal boundary was labeled and the crystal image was rotated until its boundaries were parallel to the image sides. The center of the 2-D crystal image was determined and the intensity profiles were extracted from the pixel sequences passing through the center of crystal image parallel to the crystal boundaries. The values of 3–15 pixel sequences around the central sequence for every direction were read and averaged in one-dimensional sequence to increase the signal-to-noise ratio. Intensity data from one of the two lateral directions (x or y) of different optical cuts through the crystal were used to calculate the intensity profiles in the z direction.

The thickness of the crystal was automatically determined by focusing the lens on the crystal top and at the bottom. Other crystal dimensions were determined from the position of the peaks of the 2-D intensity profiles.

RESULTS

The batch experiments were performed with different lysozyme crystal structures. Each experiment yielded 2-D images revealing the distribution of sodium fluorescein in the lysozyme crystals. Figure 3 shows a schematic drawing of the triclinic lysozyme crystal structure and the development of the fluorescence distribution in a 2-D section of the crystal as a function of depth (Fig. 3a) and time (Fig. 3b). A Cartesian coordinate system and its origin were defined for each protein crystal. In Figure 3a, the x-coordinate was chosen parallel to the short side of the image while the y-coordinate was chosen perpendicular to x along the long side. Consequently, the z-coordinate represents the direction describing the crystal thickness perpendicular to the image. The same approach was used for all crystal structures (Fig. 4).

Figure 3b shows that over a period of 60 h the fluorescent area gradually extended into the core region of the crystal. The fluorescence is proportional to the fluorescein concentration (see Discussion section), so that CLSM can be used to monitor the fluorescein penetration in a protein crystal simultaneously in x- and y-directions. Suppose that the time lag for recording images of series of sections is negligible in relation to the total time taken for the diffusion process. Then, the image series can be considered as the representative of a discrete time and allow the reconstruction of a 3-D image of the infused protein crystal. The time needed to produce a 3-D image depends on the speed of the scan and on the number of sections, and should be much smaller than the time required for fluorescein penetration in the core of the crystal. Acquisition time needed for one 2-D cut was kept the same in all experiments at 1.5 s. Considering the thickness of the triclinic lysozyme crystal in Figure 3 and the size of a pixel in horizontal sections (1.953 × 1.953 μm), 12 optical cuts were performed. The total acquisition time of 18 s for the crystal shown in Figure 3 is very short compared to the time needed for fluorescein to saturate the crystal. Therefore, 3-D images are reliable even though the 2-D scans at various depths are not taken at exactly the same instant of time. All images within a given stack are therefore effectively acquired at a discrete time.

The acquisition time should be adapted to the diffusion rate in the material. For solute transport in nonsolid materials, the diffusion process will be much faster and shorter acquisition times would be needed. For the instrument used in this study the shortest acquisition time was around 0.35 s, which would usually not be enough for monitoring diffusivity in nonsolid materials.

Intensity profiles in all three directions are presented for the tetragonal crystal structure for different time intervals (Fig. 4). All profiles are characterized by two maxima representing the penetration of the fluorescein into the crystal. The small differences in the size of maxima in Figure 4b and 4c are due to the relative position of the crystal to the incoming beam light. The 2-D cuts were always perpendicular to the laser beam. This does not imply that the cuts are parallel to the bottom and to the top faces of the crystal because the positioning of the crystal may not be flat. Additionally, it does not imply that the cuts are perpendicular to the side faces of the crystal.

The situation is different in the z direction. The main disadvantage of CLSM is its requirement for a uniform refractive

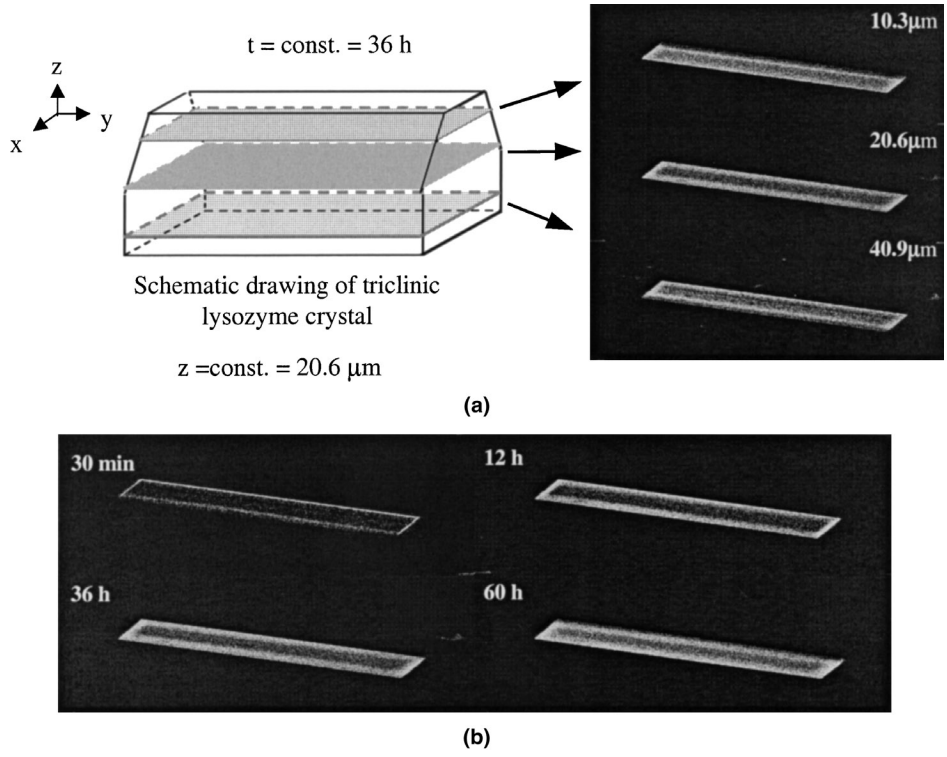

Figure 3. Confocal images of a triclinic lysozyme crystal (361.3 × 77.2 × 68.3 μm) (a) at 36 h and at different depths of the crystal; (b) at z = 20.6 μm and different times.

index over the optical path length (Booth et al., 1998; Sheppard and Torok, 1997; Visser et al., 1991). This requirement was not met in the experiments presented here. The refractive index of the lysozyme crystals and fluorescein—mother liquor solutions were 1.53–1.58 (Caylor et al., 2001; Cervelle et al., 1974) and around 1.33–1.34 (Fredericks et al., 1994), respectively. These differences were so large that by adding a versatile dipolar solvent, dimethylsulfoxide, (Kluijtmans et al., 1998) or D-glucose (Malmsten et al., 1999) to the solution, matching of the refractive indexes of solid and liquid could not be achieved in our case. The change in composition due to such additives also would make interpretation of the obtained diffusion and partitioning data a complex issue.

Due to the refractive index mismatch, the rays near the optical axis are bent to a different degree than those at large angles to the optical axis. The result is that each cone of illumination is bent to a different focal plane. The extent of this aberration depends on the numerical aperture of the objective (*NA*), the axial position of the nominal focus point within the sample and the ratio of refractive indexes of the sample (n_s) and of the objective (n_0). As a result, a change in the position of the focal point (focal shift) and a decrease in detected intensity by CLSM (Booth et al., 1998; Booth and Wilson, 2001; Diaspro et al., 2002; Hell et al., 1993; Michielsen, 2001; Sheppard and Torok, 1997; Visser et al., 1991) are detected. The latter one can easily be detected in Figure 4d where the left side maxima represent fluorescein distribution in the top crystal layer and right hand maxima represent the bottom crystal layer. The shift in the position of the focal plane cannot be directly detected from Figure 4d, but is essential for any correction of the intensity readings.

A rigorous treatment with geometric optics (Diaspro et al., 2002) leads to the following analytical solution between the distances from objective to nominal focal point (Δ_z) and from objective to the actual focal position (Δ_f) along the optical axis within the sample space:

$$\Delta_f = \frac{n_s}{n_0} \cdot \frac{\left[1 - \left(\frac{n_s}{n_0} \cdot \sin\alpha_0\right)^2\right]^{1/2}}{\cos\alpha_0} \cdot \Delta_z \qquad (1)$$

where α_0 is angle determined by objective numerical aperture (NA/n_0). By using Eq. (1), we can foresee that whenever $n_0 < n_s$ (case here) or $n_0 > n_s$, the measured axial elongation of the object is underestimated or overestimated, respectively. The z-coordinates of all experimental data and curves representing diffusion of fluorescein in the axial direction (Fig. 4d) were corrected using Eq. (1).

Considering the nonlinear character of the intensity change with an axial position of the focus (Booth et al., 1998; Booth and Wilson, 2001; Hell et al., 1993), correction of the intensity data in axial direction is relatively easy when the crystal is saturated with solute. Then, the contribution of diffusion to the intensity profiles is constant and the change in intensity is due to the refractive index mismatch in the system. Based on the saturated intensity profiles (profile in Fig. 4d for a diffusion time of 50 min) we calculated the

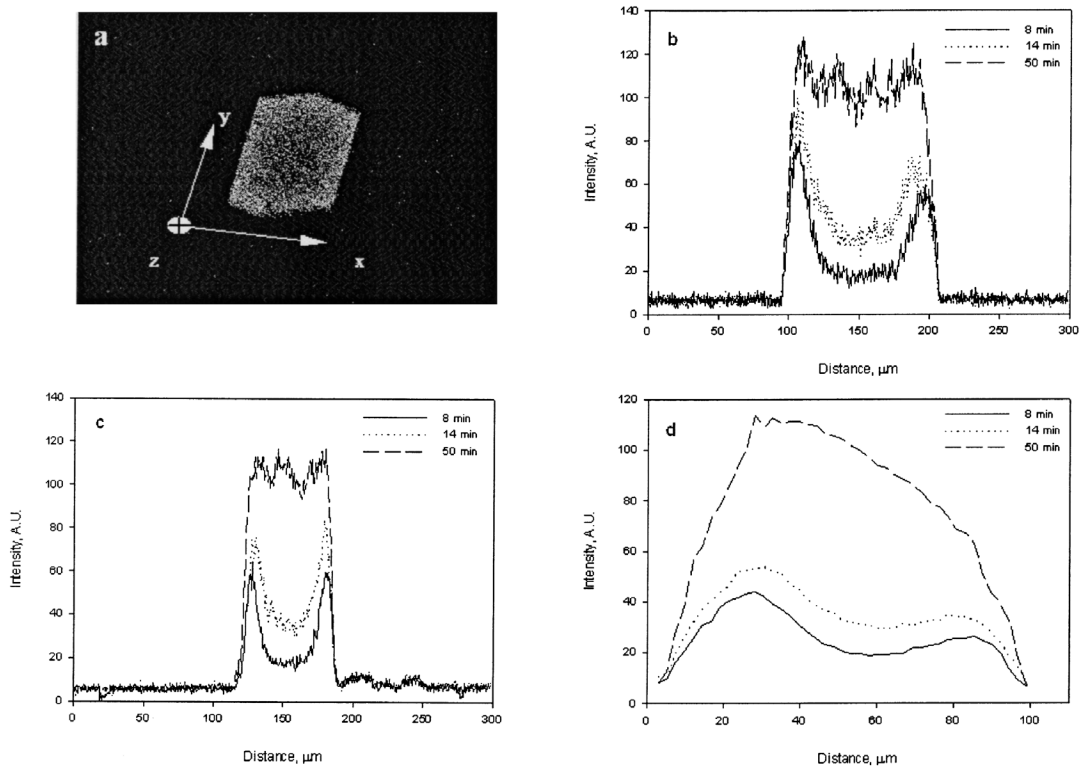

Figure 4. Fluorescence intensity profiles of tetragonal lysozyme crystal (a) (intensity in arbitrary units) in *x*-direction (b), *y*-direction (c) and *z*-direction (d).

correction factors (k_{RI}) for every z position as:

$$k_{RI}(z) = \frac{I^{sat}(z)}{I_0^{sat}} \tag{2}$$

where I_0^{sat} is the fluorescein fluorescence intensity at the top layer of the crystal (left maximum in Fig. 4d) and $I^{sat}(z)$ is the fluorescence intensity at position z in the axial direction in the saturated crystal. Then, the real diffusion profiles were calculated from the intensity profiles at various times:

$$I^{cor}(z) = \frac{I(z)}{k_{RI}(z)} \tag{3}$$

where I and I^{cor} are the measured and corrected value of intensity in the crystal at position z. As a result of this procedure experimental intensity profiles presented in Figure 4d were corrected in profiles shown in Figure 5.

Our observation that sodium fluorescein (M_w = 376.85 g/mol) penetrates the protein crystals (Fig. 3) is in line with the observations made by Pastinen et al. (2000) and Vilenchik et al. (1998) that polyethylene glycols can penetrate the protein crystals, provided that their molecular mass is below 1000. The concentration of the diffusing species, fluorescein, in bulk liquid can be considered constant because the liquid volume is more than 10^6 times larger than the volume of the crystal. The process of transport of the fluorescein into lysozyme crystals can be considered to occur in two stages: the diffusion of the dye molecules from the solution to the surface of a crystal and diffusion of the dye to the crystal center. Considering the relatively high diffusion coefficient of fluorescein in water, $0.48–0.55 \times 10^{-9}$ m^2/s (deBeer et al., 1997), we do not expect external transport limitations during fluorescein uptake by the lysozyme crystals. So, diffusion of fluorescein inside the crystal is assumed as a rate-limiting step. We assume that diffusion occurs only in the mesopore volume with a diffusion coefficient, D_e, which represents the value in free solution reduced by the effects of finite interstitial

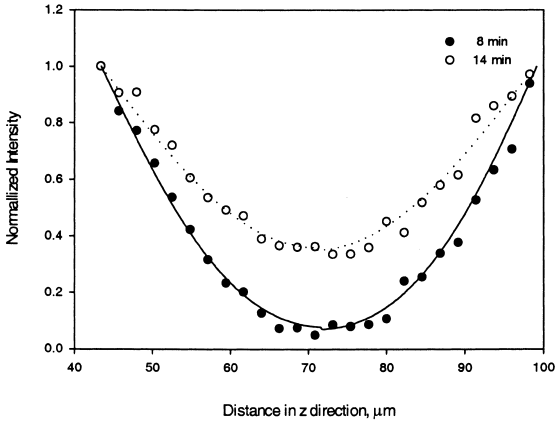

Figure 5. Experimental profiles (markers) normalized and corrected for refractive index mismatch in the system and calculated profiles (lines) for *z*-direction in the tetragonal crystal of Figure 4d.

volume, hindrance, and tortuosity (Deen, 1984; Velev et al., 2000) making it an effective diffusion coefficient considering the porosity and the tortuosity. This interstitial diffusion is coupled to fluorescein adsorption, resulting in the following diffusion equation (Velev et al., 2000):

$$\varepsilon \cdot \frac{\partial C}{\partial t} + \Phi \cdot \frac{\partial q}{\partial t} = D_e \cdot \nabla^2 C \tag{4}$$

where C is the local concentration in the pore, q the concentration of adsorbed fluorescein (per total crystal volume), ε is the crystal porosity and Φ is the specific surface area available for adsorption. Assuming that the relationship between q and C is linear for low concentrations, we get a simplified diffusion equation:

$$\frac{\partial C}{\partial t} = D_p \cdot \nabla^2 C \tag{5}$$

Here we use a pore diffusion coefficient (D_p) as a parameter, defined by

$$D_p = \frac{D_e}{\varepsilon + \Phi \cdot K} \tag{6}$$

Diffusion in the solid porous particles depends largely on the geometry of the particles, size and connectivity of the pores, etc. Effective diffusivities as described in Eq. (6) account for the effect of the pores and charge–charge interactions on the transport processes in protein crystals, but not for the geometry of the crystal. In the literature, mathematical solutions of Eq. (5) for spherical or cylindrical solid structures are available. However, neither of the lysozyme crystals geometries could be approximated as a sphere nor as a cylinder. To overcome influence of crystal geometry on the diffusion process, we calculated diffusivities separately in each orthogonal coordinate. Considering the 3-D character of the fluorescein diffusion in the protein crystal, calculating diffusivities in each orthogonal coordinate of the crystal is possible before diffusion fronts from different directions meet; since the profiles are a result of the diffusion component in that direction. Therefore, our calculations consider only intensity profiles extracted for the initial penetration time of the diffusion process. This allows us to consider diffusion along one of the crystal coordinates independent from diffusion along other coordinates and allows simplifying one 3-D transport problem into three separate 1-D transport problems according to

$$\frac{\partial C}{\partial t} = D_n \cdot \frac{\partial^2 C}{\partial n^2} \tag{7}$$

The symbol n stands for the coordinates in crystal (x, y, and z). The relatively high diffusion coefficient of fluorescein in water—0.48–0.55 $\times$ 10^{-9} m^2/s (deBeer et al., 1997)—is the direct result of low transport resistance in bulk liquid making the assumption of constant concentration of solute at the crystal surface adequate for the monitored system. Crank (1995) gives the solution of Eq. (7), for diffusion in plane sheets with constant concentration of fluorescein at the crystal surface at time t

$$\frac{C - C_0}{C_1 - C_0} = 1 - \frac{4}{\pi} \cdot \sum_{i=0}^{\infty} \left[\frac{(-1)^i}{(2i+1)} \cdot \exp\left\{ \frac{-D_n \cdot (2i+1)^2 \cdot t \cdot \pi^2}{4 \cdot L_n^2} \right\} \cdot \cos \frac{(2i+1) \cdot m \cdot \pi}{2 \cdot L_n} \right] \tag{8}$$

C_0 is the initial concentration of fluorescein in the crystal (here $C_0 = 0$), C_1 the concentration at the crystal surface (kept constant), L_n is half the distance between the crystal surfaces in the n crystal coordinate, m is the distance from the crystal center, and C is the concentration at position m. Equation (8) was used to fit experimental data for calculating D_n as shown in Figure 5. Considering the structure of Eq. (8) in the calculation only one half of the intensity profile in every direction was used. A calculation was then repeated for the other half of the intensity profile to check validity of calculated diffusivities.

An overall effective diffusion coefficient (D_{oe}) for every crystal was calculated using Hill's solution of Fick's law of diffusion for a plane sheet (Hill, 1928)

$$\frac{C_{k=0}}{C_1} = 1 - \frac{8}{\pi} \cdot \left[\exp\left(- \frac{D_{oe} \cdot \pi^2 \cdot t}{4 \cdot L_k^2} \right) + \frac{1}{9} \cdot \exp\left(- \frac{9 \cdot D_{oe} \cdot \pi^2 \cdot t}{4 \cdot L_k^2} \right) + \ldots \right] \tag{9}$$

$C_{k=0}$ is the concentration in the crystal center at time t. Equation (9) is valid for $C_{k=0} > 0$ otherwise $C_{k=0} = 0$. To approach a plane, the shortest crystal dimension, k, was selected for calculation of D_{oe}.

The average calculated values for D_{oe} and D_n of fluorescein in all lysozyme crystal structures are summarized in Table I. Per crystal structure two to three experiments were performed using different crystal sizes. The standard deviations noted in Table I indicate that the reproducibility is reasonable.

Two values for D_n are missing from Table I. In the case of triclinic crystals, the CLSM images could not be processed due to the high optical artifacts resulting from the highly tilted crystal faces. A different approach to data handling will be necessary in this case. In the case of the monoclinic crystal structure rapid penetration along the x and z coordinates disturbed the initial profiles along the y coordinate. Precisely, the profiles established in all orthogonal directions in the monoclinic crystal except the y direction were similar to the profiles presented for the tetragonal crystal in Figure 4. In the y direction of the monoclinic lysozyme crystal, flat profiles characteristic of saturated crystal were observed. Our explanation is that the diffusion in this crystal direction is too small to be measured in the presence of diffusion in the other two directions. Proof for

this hypothesis may be obtained when a 3-D diffusion model is developed and able to fit the obtained experimental data.

DISCUSSION

Transport of Fluorescein in Different Crystal Structures

Two sorts of parameters were extracted from the experimental data of fluorescein transport in lysozyme crystals (Table I). D_{oe}, commonly used as macroscopic parameter for diffusion in different media, and D_n, indicating diffusion in different directions in the crystals. Obtained values of D_{oe} were in the range from 6.2×10^{-15} to 120×10^{-15} m^2/s depending on the lysozyme crystal morphology. This might be unexpected considering that the building block for all structures is the same protein molecule, lysozyme.

Adsorption of fluorescein in lysozyme crystals, and hence D_{oe}, are expected to be influenced by pH because the charge difference between fluorescein and lysozyme is pH dependent. However, there is no correlation between D_{oe} and pH (Table I). Also, there is no correlation with crystal density or calculated solvent content (Table I). The values of D_n obtained from the confocal images showed that the transport process in all four lysozyme crystal structures is anisotropic (Table I). The level of anisotropy differs between the structures. The ratio between D_n values in any two directions generally is 1.2–5.8 showing a modest level of anisotropy, but transport in the y direction of the orthorhombic structure is 15 and 41 times higher than in x and z directions, respectively. This suggests that the orthorhombic lysozyme crystal has a highly open pore structure in the y-direction that was not expected on the basis of the crystal lattices.

The distances between the crystal planes in the lattice could not be used to explain the observed diffusion anisotropy. For example, the distances between the planes in x and z directions of the tetragonal crystal are the same but their corresponding pore diffusivities differ (Table I). In the y direction the distance is 2 times smaller than in the other two directions (data not shown), but D_y is in between D_x and D_z.

The observed anisotropy of diffusion might be explained from the apparent sizes of the pores in the crystal structures. However, the information available in the literature is limited to the tetragonal crystal's pores, which varied from 0.6 to 4 nm (Morozova et al., 1996). Considering that the size of the fluorescein molecule is around 0.9 nm, size exclusion might cause anisotropic diffusion. A preliminary attempt to reconstruct the pore network using commercially available software did not provide a conclusive correlation between diffusion coefficients and pore sizes in the crystal. Detailed analyses will be needed for a better understanding.

The anisotropy causes the D_{oe} be determined by the individual values of $D_{n.}$ This is most clear for the orthorhombic structure, where the diffusion through the top and bottom ends of the needles is much faster than through the other crystal faces. Consequently, this could influence the application of orthorhombic form of crystal. For example, orthorhombic crystal used as a biosensor would give the quickest response if one of the needle-ends is directed toward the specimen. Furthermore, the performance of orthorhombic protein crystal as catalyst or separation media could be affected by the observed anisotropy.

Limitations of the CLSM Technique for Transport Studies in Protein Crystals

There are some limitations of the CLSM technique for the study of diffusion processes in protein crystals. The limitations because of refractive index mismatch and crystal position to the incoming light in the system have been addressed in the previous discussion.

Also, the autofluorescence or the absorbance of protein crystals restricts the application of CLSM to monitor solute diffusion in protein crystals. Protein fluorescence can be caused by tryptophan, tyrosine, and phenylalanine. If excited, these amino acid residues are fluorescent in the UV region below 400 nm (Lakowicz, 1983). Therefore, experiments should not be done in the UV region. Additionally, some protein crystals show autofluorescence or absorbance in the visible part of the spectrum due to cofactors. This also limits the applicability of the present method.

In addition, protein crystals are birefringent. Birefringence characterizes the protein crystal as an anisotropic medium and can be referred to as double refraction. Maximal birefringence occurs when a ray of light traverses the crystal perpendicularly to its optical axis (Pluta, 1988). Birefringence can be neglected if the light beam is not perpendicular to the optical axis. In our experiments, laser light never entered a crystal perpendicular to its optical axis resulting in the difference between the magnitudes of the maxima in Figure 4. Therefore, we assumed that the influence of protein crystal birefringence could be neglected for our experiments.

To make quantitative measurements, we have tacitly assumed that the emitted fluorescence is proportional to the illuminating laser intensity. It has been well documented that optical saturation of a fluorophore can affect the proportionality relationship (Vissher et al., 1994). Fluorescence accumulation occurs when the exciting illumination is so intense that significant fractions of the fluorophores are in the excited state and are no longer able to respond to the incident intensity. Although the effect of fluorescence accumulation can be accounted for (Vissher et al., 1994), it has been neglected in the present study. Fluorescence saturation was avoided by working with very diluted sodium fluorescein solutions, and as photodestruction (Klonis and Sawyer, 1996) was negligible the fluorescence intensity really represented concentrations. The fluorescein concentration in the bulk liquid (0.003 mg/L) was about 1000 times smaller than the highest fluorescein concentration that still showed proportionality to fluorescence intensity for other solid materials (Burke et al., 2000; deBeer et al., 1997; Song et al., 2000), supporting the assumption that such a proportionality also occurred under our experimental conditions.

CONCLUSIONS

Confocal laser scanning microscopy allows in situ study of solute transport inside a protein crystal. This technique is relatively simple and quick. The depth-discriminating property of confocal microscopy can be used to create virtual sections through a protein crystal without destroying it. Intensity profiles, as functions of time and position can be determined. A series of 3-D pictures obtained at various times enables the calculation of concentration variations with time and space. The resulting data allow calculation of the diffusion coefficient coefficients of solutes in protein crystals. Anisotropy of the fluorescein diffusion in lysozyme crystal as a result of crystal morphology and crystals anisotropy is clearly visualized and quantified. Differences in the level of fluorescein transport between lysozyme crystal structures and the anisotropy of the transport indicate that the transport is determined by the mesoscopic crystal structure. The results presented here can help to improve understanding of the complexity of transport in mesoscopic pore structures not only of protein crystals, but also of other types of immobilized protein particles.

We are thankful to the Netherlands Institute for Metals Research for providing experimental facilities and support. We would like to thank Prof. Dr. Lucas J. van Vliet and Bernd Rieger for their help in processing of confocal images and Johan Tirell for his contribution in initializing the CLSM measurements.

References

Ahmed M, Pyle DL. 1999. Investigation of single protein adsorption on ion exchangers using confocal laser scanning microscopy. J Chem Technol Biotechol 74:193–198.

Benda A, Benes M, Marecek V, Lhotsky A, Hermens WT, Hof M. 2003. How to determine diffusion coefficients in planar phospholipid systems by confocal fluorescence correlation spectroscopy. Langmuir 19: 4120–4126.

Bishop WH, Richards FM. 1968. Properties of liquids in small pores. Rates of diffusion of some solutes in cross-linked crystals of beta-lactoglobulin. J Mol Biol 38:315–328.

Booth MJ, Wilson T. 2001. Refractive-index-mismatch induced aberrations in single-photon and two-photon microscopy and the use of aberration correction. J Biomed Opt 6:266–272.

Booth MJ, Neil MAA, Wilson T. 1998. Aberration correction for confocal imaging in refractive-index-mismatched media. J Microsc 192:90–98.

Botin AS, Morozov VN. 1985. Transfer of the low molecular weight compounds in protein crystals and films. Biofizika 32:22–28.

Burke MD, Park JO, Srinivasarao M, Khan SA. 2000. Diffusion of macromolecules in polymer solutions and gels: A laser scanning confocal microscopy study. Macromolecules 33:7500–7507.

Caylor CL, Speziale S, Kriminski S, Duffy T, Zha CS, Thorne RE. 2001. Measuring the elastic properties of protein crystals by brillouin scattering. J Cryst Growth 232:498–501.

Cervelle PB, Cesbron F, Berthou J, Jolles P. 1974. Morphologie et proprietes des cristaux de lysozyme de poule de type quadratique et orthorhombique. Acta Cryst A 30:645–648.

Crank J. 1995. Mathematics of diffusion. New York: Oxford Science Publications Clarendon Press.

deBeer D, Stoodley P, Lewandowski Z. 1997. Measurement of local diffusion coefficients in biofilms by microinjection and confocal microscopy. Biotechnol Bioeng 53:151–158.

Deen WM. 1984. Hindered transport of large molecules in liquid filled pores. AIChE J 33:1409–1425.

Diaspro A, Federici F, Robello M. 2002. Influence of refractive-index mismatch in high-resolution three-dimensional confocal microscopy. Appl Opt 41:685–690.

Diehl H. 1987. Study on fluorescein-V: The absorbance of fluorescein in the ultraviolet, as a function of pH. Talanta 34:739–741.

Doscher MS, Richards FM. 1963. The activity of an enzyme in the crystaline state: Ribonuclease S. J Biol Chem 238:2399–2406.

Feher G, Kam Z. 1985. Nucleation and growth of protein crystals: General principles and assays. Meth Enzymol 114:78–112.

Fredericks WJ, Hammonds MC, Howard SB, Rosenberger F. 1994. Density, thermal expansivity, viscosity and refractive-index of lysozyme solutions at crystal-growth concentrations. J Cryst Growth 141:183–192.

Genzel L, Keilmann F, Martin TP, Winterling G, Yacoby Y, Frohlich H, Makinen MW. 1976. Low-frequency Raman spectra of lysozyme. Biopolymers 15:219–225.

Granick S. 1942. Some properties of crystalline guinea pig hemoglobin. J Gen Physiol 25:571–578.

Hell S, Reiner G, Cremer C, Stelzer EHK. 1993. Aberrations in confocal fluorescence microscopy induced by mismatches in refractive-index. J Microsc 169:391–405.

Hill AV. 1928. The diffusion of oxygen and lactic acid through tissues. Proc R Soc London 104:39–96.

Kachalova GS, Lanina NF, Atanasov BP, Morozov VN, Shljapnikova EA, Morozova TY. 1995. The X-ray-fluorescence study of the ionic content of the lysozyme crystals. Biofizika 40:274–282.

Kim HB, Hayashi M, Nakatani K, Kitamura N, Sasaki K, Hotta JI, Masuhara H. 1996. In situ measurements of ion-exchange processes in single polymer particles: Laser trapping microspectroscopy and confocal fluorescence microspectroscopy. Anal Chem 68:409–414.

Klonis N, Sawyer WH. 1996. Spectral properties of the prototropic forms of fluorescein in aqueous solution. J Fluoresc 6:147–157.

Kluijtmans SGJM, de Hoog EHA, Philipse AP. 1998. Self-diffusion of charged colloidal tracer spheres in transparent porous glass media: Effect of ionic strength and pore size. J Chem Phys 108:7469–7477.

Lakowicz JR. 1983. Principles of fluorescence spectroscopy. New York: Plenum Press.

Linden T, Ljunglof A, Kula MR, Thommes J. 1999. Visualizing two-component protein diffusion in porous adsorbents by confocal scanning laser microscopy. Biotechnol Bioeng 65:622-630.

Ljunglof A, Thommes J. 1998. Visualising intraparticle protein transport in porous adsorbents by confocal microscopy. J Chrom A 813:387–395.

Ljunglof A, Larsson M, Knuuttila KG, Lindgren J. 2000. Measurement of ligand distribution in individual adsorbent particles using confocal scanning laser microscopy and confocal micro-raman spectroscopy. J Chrom A 893:235–244.

Lowry M, He Y, Geng L. 2002. Imaging solute distribution in capillary electrochromatography with laser scanning confocal microscopy. Anal Chem 74:1811–1818.

Malmsten M, Xing KZ, Ljunglof A. 1999. Confocal microscopy studies of trypsin immobilization on porous glycidyl methacrylate beads. J Colloid Interface Sci 220:436–442.

Margolin AL, Navia MA. 2001. Protein crystals as novel catalytic materials. Angew Chem Int Ed 40:2205–2222.

Matthews BW. 1968. Solvent content of protein crystals. J Mol Biol 33: 491–497.

McRee D. 1999. Practical protein crystallography. San Diego: Academic Press. 187 p.

Michielsen S. 2001. Aberrations in confocal spectroscopy of polymeric materials: Erroneous thicknesses and intensities, and loss of resolution. J Appl Polym Sci 81:1662–1669.

Morozov VN, Morozova TY. 1992. Mechanical detection of interaction of small specific ligands with proteins and DNA in cross-linked samples. Anal Biochem 201:68–79.

Morozov VN, Kachalova GS, Evtodienko VU, Lanina NF, Morozova TY.

1995. Permeability of lysozyme tetragonal crystals to water. Eur Biophys J 24:93–98.

Morozova TY, Kachalova GS, Lanina NF, Evtodienko VU, Botin AS, Shlyapnikova EA, Morozov VN. 1996. Ionic conductivity, transference numbers, composition and mobility of ions in cross-linked lysozyme crystals. Biophys Chem 60:1–16.

O'Hara P, Goodwin P, Stoddard BL. 1995. Direct measurement of diffusion rates in enzyme crystals by video absorbance spectroscopy. J Appl Cryst 28:829–834.

Pastinen O, Visuri K, Leisola M. 1998. Xylitol purification by cross-linked glucose isomerase crystals. Biotechnol Tech 12:557–560.

Pastinen O, Jokela J, Eerikainen T, Schwabe T, Leisola M. 2000. Cross-linked glucose isomerase crystals as a liquid chromatographic separation material. Enzyme Microb Technol 26:550–558.

Pluta M. 1988. Advanced light microscopy. Principles and basic properties. Amsterdam: Elsevier.

Rademann J, Barth M, Brock R, Egelhaaf HJ, Jung G. 2001. Spatially resolved single bead analysis: Homogeneity, diffusion, and adsorption in cross-linked polystyrene. Chem Eur J 7:3884–3889.

Reichert U, Linden T, Belfort G, Kula MR, Thommes J. 2002. Visualising protein adsorption to ion-exchange membranes by confocal microscopy. J Membr Sci 199:161–166.

Rupley JA. 1969. The comparison of protein structure in the crystal and in solution (pp. 291–352). In: Timasheff SN, Fasman GD (eds.). Structure and stability of biological macromolecules. New York: Marcel Dekker Inc.

Sheppard CJR, Torok P. 1997. Effects of specimen refractive index on confocal imaging. J Microsc 185:366–374.

Sluyterman LAA, de Graaf MJ. 1969. The activity of papain in the crystalline state. Biochim Biophys Acta 171:277–287.

Song Y, Srinivasarao M, Tonelli A, Balik CM, McGregor R. 2000. Laser scanning confocal microscopy study of dye diffusion in fibers. Macromolecules 33:4478–4485.

St Clair NL, Navia MA. 1992. Cross-linked enzyme crystals as robust biocatalysts. J Am Chem Soc 114:7314–7316.

Steinrauf LK. 1959. Preliminary X-ray data for some new crystalline forms of B-lactoglobulin and hen egg-white lysozyme. Acta Cryst 12: 77–79.

Velev OD, Kaler EW, Lenhoff AM. 2000. Surfactant diffusion into lysozyme crystal matrices investigated by quantitative fluorescence microscopy. J Phys Chem B 104:9267–9275.

Vilenchik LZ, Griffith JP, St Clair N, Navia MA, Margolin AL. 1998. Protein crystals as novel microporous materials. J Am Chem Soc 120: 4290–4294.

Visser TD, Groen FCA, Brakenhoff GJ. 1991. Absorption and scattering correction in fluorescence confocal microscopy. J Microsc 163: 189–200.

Vissher K, Brakenhoff GJ, Visser TD. 1994. Fluorescence saturation in confocal microscopy. J Microsc 175:162–165.

Westbrook EM, Sigler PB. 1984. Enzymatic function in crystals of delta 5-3-ketosteroid isomerase. Catalytic activity and binding of competitive inhibitors. J Biol Chem 259:9090–9095.